Robust Spoofing Detection and Mitigation based on Direction of Arrival Estimation

Manuel Appel*, Andriy Konovaltsev*, Michael Meurer *†
* Institute of Communications and Navigation, German Aerospace Center (DLR), Oberpfaffenhofen, Germany
manuel.appel@dlr.de, andriy.konovaltsev@dlr.de † Chair of Navigation, RWTH Aachen University, Germany
michael.meurer@nav.rwth-aachen.de

BIOGRAPHY

Manuel Appel received his diploma degree in electrical engineering from the university of applied science Ingolstadt, Germany in 2008. Additionally he received a M.Sc. degree from Technical University Munich in 2013 after working at Fraunhofer Institute for Integrated Circuits in Erlangen. He joined the Institute for Communication and Navigation of DLR in January 2014. His main research interest is in development of signal processing algorithms for robust GNSS receivers with the main focus on spoofing detection and mitigation.

Andriy Konovaltsev received his engineer diploma and the Ph.D. degree in electrical engineering from Kharkov State Technical University of Radio Electronics, Ukraine in 1993 and 1996, respectively. He joined the Institute of Communications and Navigation of DLR in 2001. His main research interest is in application of antenna array signal processing for improving performance of satellite navigation systems in challenging signal environments.

Michael Meurer received the diploma in electrical engineering and the Ph.D. degree from the University of Kaiserslautern, Germany. After graduation, he joined the Research Group for Radio Communications at the Technical University of Kaiserslautern, Germany, as a senior key researcher, where he was involved in various international and national projects in the field of communications and navigation both as project coordinator and as technical contributor. From 2003 till 2013, Dr. Meurer was active as a senior lecturer and Associate Professor (PD) at the same university. Since 2006 Dr. Meurer is with the German Aerospace Centre (DLR), Institute of Communications and Navigation, where he is the director of the Department of Navigation and of the center of excellence for satellite navigation. In addition, since 2013 he is a professor of electrical engineering and director of the Chair of Navigation at the RWTH Aachen University. His current research interests include GNSS signals, GNSS receivers, interference and spoofing mitigation and navigation for safety-critical applications.

INTRODUCTION

The robust and reliable determination of a user position and time is crucial for civil GNSS applications with safety content, such as aircraft landing or maritime navigation in a harbor. Also many strategically important infrastructures, such as electric power grids or mobile communications networks, are becoming increasingly dependent on GNSS services. The so called spoofing-threat, i.e. transmission of a fake signal to intentionally fool receiver measurements, became a prominent subject of study in the community during the past years. In contrast to military GNSS users which solve the spoofing problem to a large extent by utilizing encrypted signals, civil users have to live today, and most probably in the near and mid future, with unencrypted signals of open GNSS services. The vulnerability of several commercial civil state-of-the-art receivers has been exploited in [1]. Users of such receivers can benefit strongly from additional receiver-sided techniques, which are able to detect and mitigate spoofing attacks.

Adequate solutions for the GNSS spoofing problem are the subject of intensive research. A number of receiver-autonomous spoofing detection techniques have been proposed, see for example [2], [3], [4] and references herein. In order to detect the presence of a spoofing attack these techniques rely on the observation of the signal power, the Doppler frequency offset, the PRN code delay and its change rate, the correlation function shape as well as the cross-correlation of the signal components at different carrier frequencies. Advanced protection against even the most sophisticated spoofing attacks can be provided by the use of multiple antennas. This comes from the fact that the carrier phases of a signal, observed at different antennas, depend on the direction of arrival of the signal [5]. Using this, a receiver with an antenna array is able to estimate the directions of arrival of the GNSS signals and detect the spoofing attack, as long as a large part of the signals come from a single direction. Moreover the malicious signals can be mitigated by generating a spatial zero in the array antenna reception pattern in the direction of the spoofing source.

The use of the multi-antenna based approach for spoofing detection and mitigation was investigated by the authors in [6] and [7]. A technique for joint spoofing detection and antenna attitude estimation by using estimated signal directions of arrival was developed. This technique was implemented in an experimental receiver [8] with an adaptive antenna array where the direction-of-arrival (DoA) is estimated for each tracking channel at the post-correlation stage. On the one hand DoA information is used to constrain the digital beamforming process. On the other hand the proposed technique uses this information also for detection of spoofing attacks. The detection is based on testing the observed DoAs of the satellite signals against the predicted DoAs. The latter are obtained in the local east-north-up (ENU) coordinates while solving the PVT problem and using the computed satellite positions and user position solution. Because the attitude of the antenna array in the local ENU coordinates is not necessarily known, the spoofing detection is therefore treated as a joint detection (i.e. of the spoofing attack) and estimation (i.e. of the attitude) problem. It was practically demonstrated that the observed DoAs can be used to identify the direction of the spoofing source and produce a spatial null in the array reception pattern for mitigating this type of radio frequency

interference.

However the technique developed in [6] and [7] still suffers from the effects of short-term inaccuracies in the direction of arrival estimation occurring during the spoofing attack. On the one hand the algorithm itself can be improved by advanced techniques. On the other hand this problem can be effectively solved by using a sequential estimation approach for the array attitude combined with an adequate user motion model. The results of practical tests reported in [7] also indicate that the DoA estimation performance under spoofing attack should be improved in order to maintain reliable spoofing detection and to point a spatial null toward the spoofing source.

This paper presents the results of an investigation aimed at the improvement of the robustness of the joint attitude estimation and spoofing detection by utilizing a sequential approach for solving the estimation problem. First an updated mathematical model for the DoA-based attitude estimation is proposed in Section I. Further in Section II a closed-form solution for this problem by using singular value decomposition (SVD) is formulated. Later in Section III the inspection of the obtained singular values is explored for the detection of anomalies in the DoA measurements. Using the results presented in Sections II and III, a snapshot-based approach for joint attitude estimation and spoofing detection is presented in Section IV. The proposed approach for the extension from the snapshot-based to the sequential attitude estimation is described in Section V. The assessment of the practical performance of the proposed sequential estimation approach by using realistic field test data is performed in Section VI. Some conclusions and outlook which are given in the last Section VII conclude the paper.

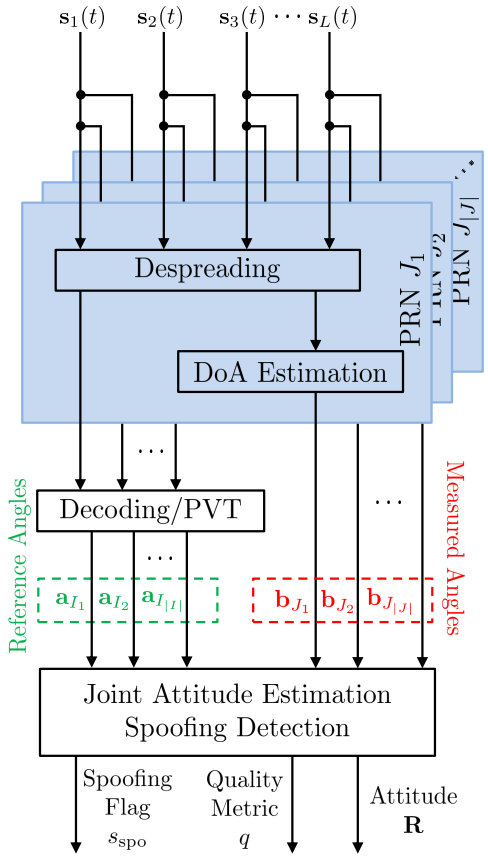

Fig. 1: Blockdiagram of the generic system setup

System Description

The system under consideration utilizes an antenna array. This enables the receiver to estimate the elevation and azimuth of the tracked and de-spreaded GNSS ranging signals separately. The navigation messages decoding and the PVT calculation are assumed to be available. Fig. 1 shows the generic system setup.

The goal of this research is to get a reliable estimate of the receivers attitude w.r.t. to a local east-north-up coordinate frame. The corresponding signal model and estimation algorithm are described in this section. A detailed derivation is presented since a deeper analysis of the attitude estimation problem automatically leads to detection schemes for anomalies which can be used for spoofing mitigation.

The measured sets of direction of arrivals (azimuth and elevation) are transformed into unit vectors pointing from the user to the satellites. These are denoted by $\boldsymbol{b}_j \in \mathbb{R}^3$ and collected in the set $\mathcal{B} = \{\boldsymbol{b}_j\}_{j \in J}$. They are represented in a local antenna coordinate system (details can be found in [9]). J denotes the set of corresponding PRN-numbers of satellites with available measurements.

A GNSS receiver capable of performing a PVT-solution is also able to calculate unit vectors pointing from the user to the satellites using ephemeris information. The single vectors $\boldsymbol{a}_i \in \mathbb{R}^3$ are collected in the set $\mathcal{A} = \{\boldsymbol{a}_i\}_{i \in I}$. These vectors are represented in a local east-north-up coordinate frame. I denotes the set of PRN numbers, which are evaluated by the receiver. If it is assumed that the almanac information is available for all tracked satellites J is a subset of I.

The local antenna coordinate frame is a rotated version of the local geodetic east-north-up frame. This yields the following equation for all available pairs of measurements $K = J \cap I$ for the error free case:

$$\boldsymbol{b}_k = \boldsymbol{R}\boldsymbol{a}_k \quad \forall k \in \mathcal{K} \tag{1}$$

The rotation is described by a rotation matrix $\boldsymbol{R} \in \mathcal{SO}(3)$ (see [10], $\mathcal{SO}(n) = \{\boldsymbol{X} \in \mathbb{R}^{n \times n} | \boldsymbol{X}\boldsymbol{X}^T = \boldsymbol{I} \wedge \det(\boldsymbol{X}) = 1\}$). It contains the information about roll, pitch and yaw and therefore defines the current attitude. This rotation (i.e. attitude) is a property of the GNSS receiver at a certain time instant and therefore is common for all pairs of unit vectors.

Measurement Model

Since the change in the user position is very small compared to the distance of the user to the satellite, the ephemeris based DoAs $\{\boldsymbol{a}_i\}_{i \in \mathcal{I}}$ are assumed to be perfectly known. The antenna array based measurements however suffer from imperfections. In [9] these imperfections are modeled by using additive Gaussian noise ($\boldsymbol{n}_k \sim \mathcal{N}(\boldsymbol{0}, \sigma\boldsymbol{I})$), yielding:

$$\boldsymbol{b}_k = \boldsymbol{R}\boldsymbol{a}_k + \boldsymbol{n}_k \quad \forall k \in K \tag{2}$$

It is remarkable that if the corresponding vectors $\boldsymbol{a}_k$ and $\boldsymbol{b}_k$ are unit vectors and both are rotated versions of each other, in a strict sense Eq.(2) cannot hold without further restrictions on the noise.

Since the noise affects the estimated angle of arrival, it seems convenient to model it using rotation matrices as well:

$$\boldsymbol{b}_k = \boldsymbol{R}_k \underbrace{\boldsymbol{R}\boldsymbol{a}_k}_{\boldsymbol{a}_k'} \quad \forall k \in K \tag{3}$$

This rotational noise $\boldsymbol{R}_k$ affects all measurements differently. The rotation matrix can be constructed choosing a random rotation axis $\boldsymbol{\omega}_k$ and choosing a random rotation angle α_k for each measurement.

Snapshot based problem statement

The ultimate goal of the algorithm is to perform a computation of the rotation matrix (which corresponds to the current attitude) and to detect anomalies in the DoA measurements (which could be caused by "spoofing" or meaconing).

Using the noise model described in Eq.(3), the following set of equations for the $N = |K|$ different pairs of measurements can be stated:

$$\begin{aligned} \boldsymbol{b}_1 &= \boldsymbol{R}_1 \boldsymbol{R}\boldsymbol{a}_1 \\ &\vdots \\ \boldsymbol{b}_k &= \boldsymbol{R}_k \boldsymbol{R}\boldsymbol{a}_k \\ &\vdots \\ \boldsymbol{b}_N &= \boldsymbol{R}_N \boldsymbol{R}\boldsymbol{a}_N \end{aligned} \tag{4}$$

In the following, $\boldsymbol{B} \in \mathbb{R}^{3\times N}$ and $\boldsymbol{A} \in \mathbb{R}^{3\times N}$ denote matrices consisting of the available DoAs in their columns. Following the maximum likelihood principle, one is interested to minimize the noise of the measurement rotation. Therefore the distance of the rotated versions of $\boldsymbol{R}_k\boldsymbol{a}_k$ and the unaffected ones $\boldsymbol{a}_k$ is to be minimized.

Since the noisy rotations are assumed to be independent for different unit vectors, a measure $g(\cdot)$ for this distance is employed for each unit vector. The results are summed up, yielding the following cost function for the antennas attitude:

$$f(\boldsymbol{R}) = \sum_{k=1}^{N} g \quad \underbrace{(\boldsymbol{R}\boldsymbol{a}_k - \boldsymbol{b}_k)}_{\text{Difference caused by noise}} \tag{5}$$

Using the squared ℓ_2-norm for $g(\cdot)$ the following ML-based optimization problem can be stated:

$$\boldsymbol{R}^* = \arg \min_{\boldsymbol{R}\in\mathcal{SO}(3)} \|\boldsymbol{R}\boldsymbol{A} - \boldsymbol{B}\|^2 \tag{6}$$

Other possible choices for $g(\cdot)$ can be found in [10] by constructing the induced norms from the metrics described therein.

Closed form solution

In [9] an iterative approach was used to solve the problem stated in 6. In the following section a closed form solution is derived, allowing further insight in the geometric properties and conditioning of the problem.

The side condition $\boldsymbol{R} \in \mathcal{SO}(3)$ is a more special case of $\boldsymbol{R} \in \mathcal{O}(3)$ ($\mathcal{O}(n) = \{\boldsymbol{X} \in \mathbb{R}^{n\times n} | \boldsymbol{X}^T\boldsymbol{X} = \boldsymbol{I}\}$). Since the latter condition implies 6 equalities due to symmetry (the diagonal elements of $\boldsymbol{R}\boldsymbol{R}^T$ to be one and the other ones to be zero), a compact version using a matrix $\Lambda \in \mathrm{Sym}(3) = \{\boldsymbol{X} \in \mathbb{R}^{3\times3} | \boldsymbol{X} = \boldsymbol{X}^T\}$ can be stated as follows:

$$h(\boldsymbol{R}) = \mathrm{tr}(\boldsymbol{\Lambda}(\boldsymbol{R}\boldsymbol{R}^T - \boldsymbol{I})) = 0 \tag{7}$$

$\boldsymbol{\Lambda}$ collects the Lagrange Multipliers. By constructing $h(\cdot)$ as stated above, all six equality constraints are summed up. Setting this sum to zero is a more relaxed but still necessary condition compared to stating them separately. The Lagrange cost function reads:

$$L(\boldsymbol{R}, \boldsymbol{\Lambda}) = \|\boldsymbol{R}\boldsymbol{A} - \boldsymbol{B}\|^2 + \mathrm{tr}(\boldsymbol{\Lambda}(\boldsymbol{R}\boldsymbol{R}^T - \boldsymbol{I})) \tag{8}$$

Following the common approach, the gradient w.r.t. $\boldsymbol{R}$ reads:

$$\frac{1}{2}\nabla_R L(\boldsymbol{R}, \boldsymbol{\Lambda}) = \underbrace{\boldsymbol{R}(\boldsymbol{A}\boldsymbol{A}^T + \boldsymbol{\Lambda})}_{\text{lhs}} - \underbrace{\boldsymbol{B}\boldsymbol{A}^T}_{:=\boldsymbol{C}=\text{rhs}} = \boldsymbol{0} \tag{9}$$

The side condition ($\boldsymbol{R}$ to be orthogonal) can be used in a tricky way to solve for $\boldsymbol{\Lambda}$. The transpose of the right hand side (rhs) of the above equation is multiplied from the left. The term containing $\boldsymbol{R}$ cancels out. The remaining term in brackets is symmetric (due to the redundancy in $\boldsymbol{\Lambda}$). The result reads:

$$(\boldsymbol{A}\boldsymbol{A}^T + \boldsymbol{\Lambda}) = (\boldsymbol{C}^T\boldsymbol{C})^{\frac{1}{2}} \tag{10}$$

Combining this result with Eq. 9 yields:

$$\boldsymbol{R}(\boldsymbol{C}^T\boldsymbol{C})^{\frac{1}{2}} = \boldsymbol{C} \tag{11}$$

Using a singular value decomposition for $\boldsymbol{C} := \boldsymbol{U}\boldsymbol{\Sigma}\boldsymbol{V}^T$ the result can be further simplified. Due to the properties of $\boldsymbol{U}$ and $\boldsymbol{V}$ (both in $\mathcal{O}(3)$) the following result can be stated:

$$\boldsymbol{R}\boldsymbol{V}\boldsymbol{\Sigma} = \boldsymbol{U}\boldsymbol{\Sigma} \tag{12}$$

To finally solve for $\boldsymbol{R}$ the matrix $\boldsymbol{\Sigma} = \mathrm{diag}(\sigma_1, \sigma_2, \sigma_3)$, has to be further investigated. Without loss of generality, the singular values are ordered decreasingly. Three cases can be distinguished, since if at least one measurement is available, the minimum rank of $\boldsymbol{C}$ is one.

1) All singular values are unequal to 0:
$\boldsymbol{\Sigma}$ is invertible. The result for $\boldsymbol{R}$ reads:

$$\boldsymbol{R}' = \boldsymbol{U}\boldsymbol{V}^T \tag{13}$$

To ensure that a proper rotation matrix (the constraint $\det(\boldsymbol{R}) = 1$ was not taken into account so far) is derived, the following "normalization" has to be performed:

$$\boldsymbol{R} = \boldsymbol{U}\mathrm{diag}(1, 1, \det(\boldsymbol{U}\boldsymbol{V}^T))\boldsymbol{V}^T \tag{14}$$

2) One singular value is equal to 0:
This corresponds to the case, where the set of $\{\boldsymbol{a}_k\}_{k=1}^N$ or $\{\boldsymbol{b}_k\}_{k=1}^N$ span only 2 dimensions. Since the goal of the optimization is to rotate one coordinate system onto the

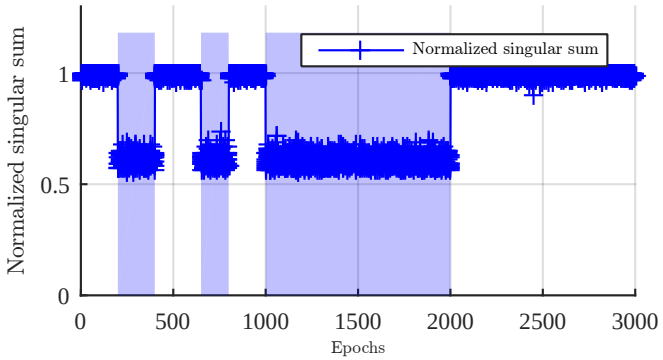

Fig. 2: Sum of Singular Value based detection of anomalies with noisy measurements (noise variance is 10 degree^2)

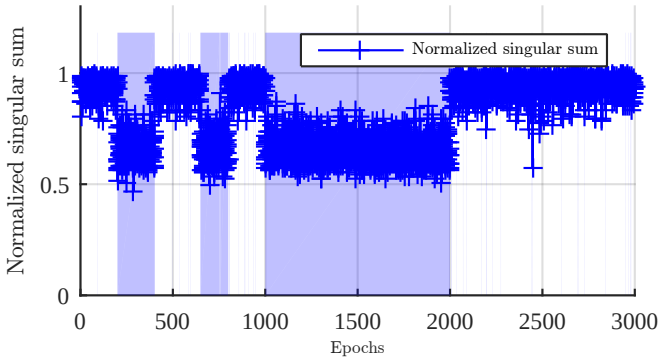

Fig. 3: Sum of Singular Value based detection of anomalies with noisy measurements (noise variance is 25 degree^2)

other, this information is enough, since the missing one is uniquely determined. The result for $\boldsymbol{R}$ therefore is the same as in previous case.

3) Two singular values are equal to 0:
This case occurs, if only one direction is present in either $\{\boldsymbol{a}_k\}_{k=1}^N$ or $\{\boldsymbol{b}_k\}_{k=1}^N$. If more than one measurement is available, this is very unlikely for the almanac data. If the measurements however span only one dimension, an anomaly is very likely, which makes an attitude determination impossible.

Anomaly Detection

As stated in the previous section, an inspection of the singular values of $\boldsymbol{C} = \boldsymbol{B}\boldsymbol{A}^T$ can be used to detect anomalies. Different possible methods are described in the following section.

Sum of Singular Values

Since the vectors are normalized to one, the sum of all singular values in the noise free case is equal to the size of $N = |K| = |I \cap J|$. This property can be used for inspection: In the case of noisy measurements, the normalized sum can be computed, yielding values from 0 to 1. If the resulting metric is below a certain threshold $\tau_{\text{sum,sing}}$ an anomaly is very likely. Fig. 2 depicts an example with moderate noise, where the approach works. A blue background indicates the groundtruth. A raised flag indicates the detection.

Fig. 3 depicts simulated results with higher noise (a variance of 25 degree), where the same threshold was used. Due to the noise, a reliable detection cannot be performed anymore. The same epochs were used for turning the spoofer on (indicated by the black background again). The detection-flag is indicated in blue.

Comparison with Almanac Geometry

On the one hand, the ratio of the singular values of $\boldsymbol{C}$ depends on the presence of a spoofer or repeater, i.e. if all measured unit vectors $\boldsymbol{b}_j$ are collinear, only one singular value is big compared to the others. On the other hand also the geometry of the almanac DoAs determines this ratio.

Therefore a comparison of the singular values of $\boldsymbol{C}_B = \boldsymbol{B}\boldsymbol{B}^T := \boldsymbol{V}_B\boldsymbol{\Sigma}_B\boldsymbol{V}_B^T$ with the ones of the geometry only

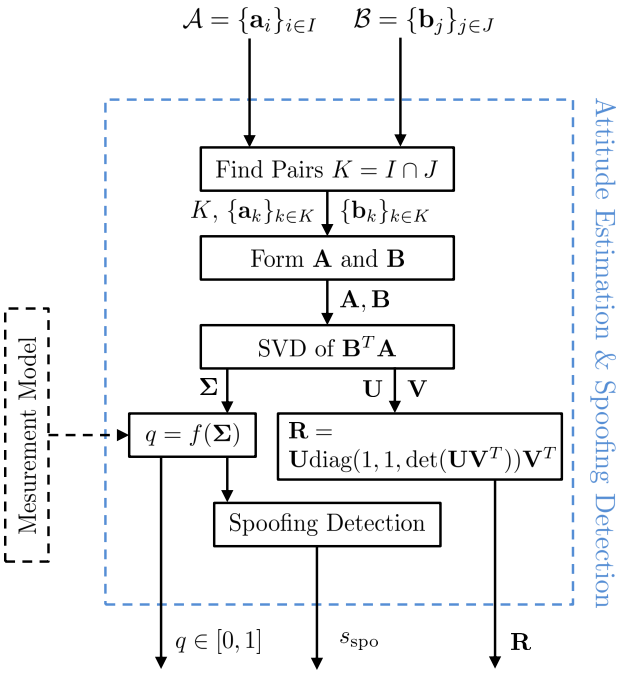

Fig. 4: Block diagram of the basic snapshot based algorithm

matrix $\boldsymbol{C}_A = \boldsymbol{A}\boldsymbol{A}^T := \boldsymbol{V}_A\boldsymbol{\Sigma}_A\boldsymbol{V}_A^T$ seems a valid candidate for indicating the presence of an anomaly.

The difference of the singular values of $d_i = \frac{1}{N}|\sigma_{A,i} - \sigma_{B,i}|$ can be used to compare the subspaces and identify the affected ones. If a subspace is identified, the corresponding singular vector (either for the almanac or the coordinate frame) can be used directly, since it reflects the repeaters direction.

Snapshot based Attitude Estimation

A block diagram of the basic snapshot based algorithm is depicted in Fig. 4. Additionally, the algorithm returns a quality metric q ranging from 0 to 1 and an indication about spoofing by generating a flag s_{spo} by using one of the previously described methods.

First the performance is analyzed using simulated data sets. A random almanac consisting of N unit vectors is generated. Afterwards a random attitude is generated by choosing a unit vector for the rotation axis and a scalar rotation angle

randomly. The almanac unit vectors are then rotated by this attitude, yielding $\{\boldsymbol{b}_k^{\text{perf}}\}_{k=1}^N$. Finally the measurements are generated by again generating a random rotation (with the constraint, that the rotation axis is orthogonal to $\boldsymbol{b}_k$).

Optionally a spoofer can be turned on for specified simulation runs. This will affect the measured signals to be arriving all from the same direction, before noise is added. For the described examples, the affected simulations are the ones in the intervals $[200, 400]$, $[650, 800]$ and $[1000, 1500]$.

Fig. 5 shows some exemplary results for 2000 different runs using a noise variance of 5 and 6 reference angles. Fig. 5 shows the same setup for only 3 almanac measurements. The runs where a spoofer was active are indicated by a blue background.

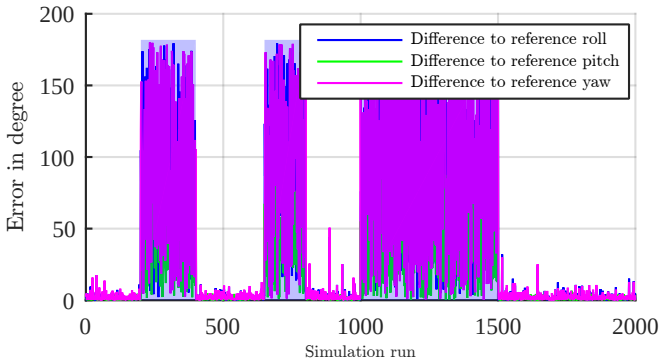

Fig. 5: Difference to reference for roll, pitch and yaw in degree; The noise variance was 5 degree^2 and $N = 6$

Fig. 6 depicts the resulting normalized singular values for this example.

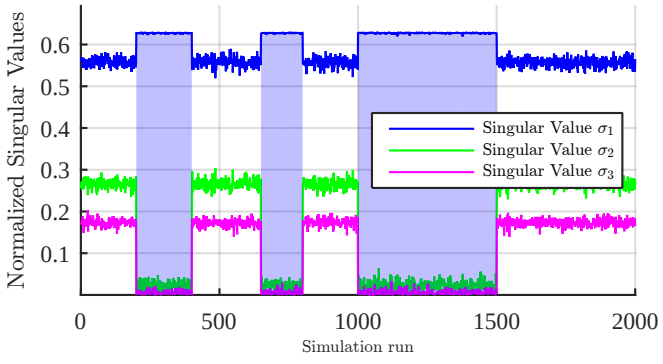

Fig. 6: Normalized singular values of $\boldsymbol{C}$; The noise variance was 5 degree^2 and $N = 6$

Fig. 7 shows the resulting SVD based metric and the detection flag.

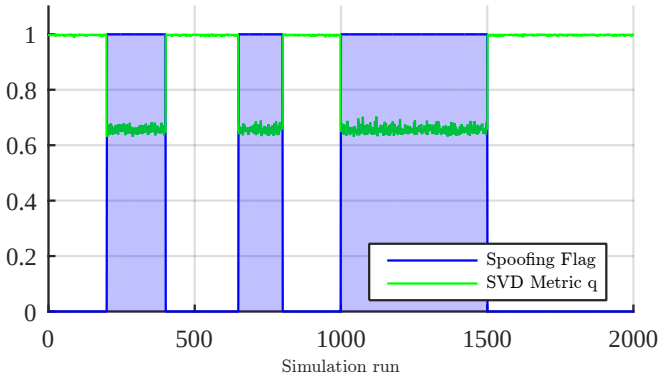

Fig. 7: Quality metric and returend spoofing flag; The noise variance was 5 degree^2 and $N = 6$

Again 2000 runs were performed using only 3 signals with a three times higher noise variance of 15 degree. Fig. 8 shows the resulting error of the attitude angles compared to the reference. The number of signals is to low to perform an estimate with such a big noise.

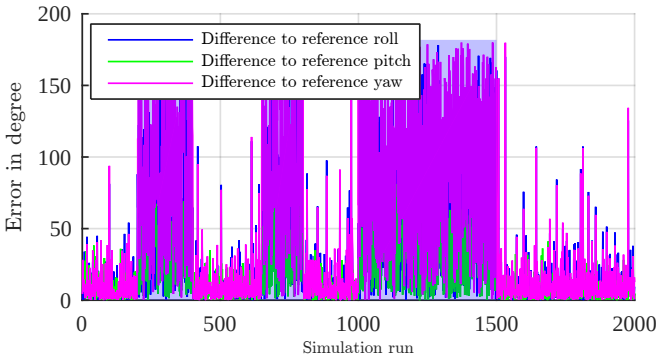

Fig. 8: Difference to reference for roll, pitch and yaw in degree; The noise variance was 15 degree^2 and $N = 3$

Fig. 9 depicts the corresponding singular values. When spoofing is active, σ_2 again almost vanishes, but not completely due to the noise.

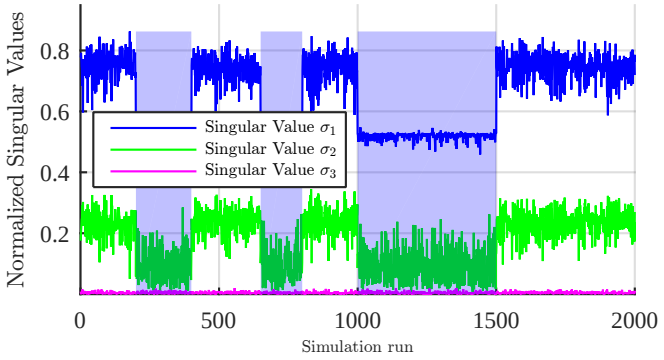

Fig. 9: Normalized singular values of $\boldsymbol{C}$; The noise variance was 15 degree^2 and $N = 3$

Spoofing detection is still almost always reliably possible, as depicted in Fig. 10.

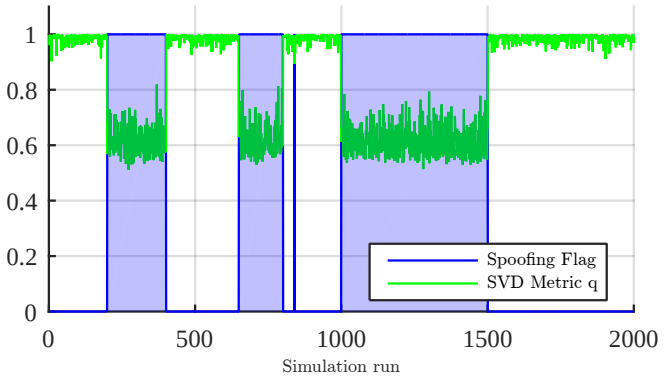

Fig. 10: Quality metric and returend spoofing flag; The noise variance was 15 degree^2 and $N = 3$

Sequential Attitude Estimation

Having a sequence of measurements for the direction of arrivals for each tracked PRN ($\mathcal{B}(n)$), it is convenient that they follow a random process, i.e. for different time instances n they are not independent. This fact can be used to gain more robust estimates of the underlying attitude of the platform denoted by $\boldsymbol{R}(n)$ compared to a snapshot based approach. In order to be able to realize a sequential estimator, states and measurements have to be defined. [7] used a simple Kalman Filter, whereas in the following a different approach will be described.

A. First order Movement Model

A first order movement model is considered first to describe the evolution of the platforms attitude over discrete time instances n. The model is defined as follows:

$$\boldsymbol{R}(n+1) = \boldsymbol{R}_N(n)\boldsymbol{R}(n) \tag{15}$$

$\boldsymbol{R}_N(n)$ denotes a random rotation matrix. It is constructed using an arbitrary rotation axis $\boldsymbol{\omega}(n)$ with $\|\boldsymbol{\omega}(n)\| = 1$ and a certain rotation angle $\alpha(n) \sim \mathcal{N}(0, \sigma_\alpha)$. The rotation matrix can then be constructed using Rodrigues' formula $(\boldsymbol{R}(\boldsymbol{\omega}, \alpha) = \boldsymbol{I} + \sin(\alpha)[\boldsymbol{\omega}]_x + (1 - \cos(\alpha))[\boldsymbol{\omega}]_x^2)$.

B. Second order Movement Model

An extension is added to the first order model to be able to describe the tendency of rotation. Therefore the rotation axis is not allowed to change arbitrary between the time instances. The change in rotation is again modeled by a random rotation matrix matrix $\boldsymbol{R}_{N_\omega}(n)$. This matrix will be randomly chosen from $\mathcal{SO}(3)$.

$$\boldsymbol{\omega}(n+1) = \boldsymbol{R}_{N_\omega}\boldsymbol{\omega}(n) \tag{16}$$

Also due to conservation of energy which corresponds to the angular velocity, the current pose angle $\alpha(n)$ is not allowed to change arbitrary. This can be modeled as follows:

$$\alpha(n+1) = \alpha(n) + \eta_\alpha(n) \tag{17}$$

Again using Rodriguez Formula yielding $\boldsymbol{R}_{N_\omega}(n)$, a random state transition reads:

$$\boldsymbol{R}(n+1) = \boldsymbol{R}_{N_2}(n)\boldsymbol{R}(n) \tag{18}$$

C. Simple Constrained Based Approach

Both movement models constrain the change of the platforms attitude for two successive time instances. A certain cost function $\Phi(\cdot,\cdot)$ is used to measure this distance. In [10] different proper metrics are discussed. The following one is used for the described approach:

$$\Phi(\boldsymbol{R}(n+1), \boldsymbol{R}(n)) = \|\boldsymbol{R}(n+1) - \boldsymbol{R}(n)\|^2 \tag{19}$$

This cost function is added to the original cost function by a trade-off parameter ϵ, which "weights" both objectives:

$$\begin{aligned}\boldsymbol{R}(n+1)^* = &\arg \min_{\boldsymbol{R}(n+1)\in\mathcal{SO}(3)} \frac{1}{N}\|\boldsymbol{R}(n+1)\boldsymbol{B} - \boldsymbol{A}\|^2 \\ &+ \epsilon\|\boldsymbol{R}(n+1) - \boldsymbol{R}(n)\|^2\end{aligned} \tag{20}$$

Using the same technique as for the snapshot based approach, the final solution is given by:

$$\boldsymbol{R}(n+1) = \boldsymbol{U}_s \mathrm{diag}(1, 1, \det(\boldsymbol{U}_s\boldsymbol{V}_s^T))\boldsymbol{V}_s^T \tag{21}$$

$\boldsymbol{U}_s$ and $\boldsymbol{V}_s$ denote the corresponding matrices of the singular value decomposition of $\boldsymbol{C}_s = \boldsymbol{U}_s\boldsymbol{\Sigma}_s\boldsymbol{V}_s^T$, where $\boldsymbol{C}_s = \frac{1}{N}\boldsymbol{B}\boldsymbol{A}^T + \epsilon\boldsymbol{R}(n)$ now includes the estimate of the previous time instant.

Finally the objective function consists of a "data fit" term and a "regularization" term. This approach is commonly used in image processing techniques (i.e. optical flow estimation). Additional smoothness constraints may be added (e.g. constraints on the change rate of the attitude to incorporate the dynamics of the second order movement model).

When employing the overall algorithm depicted in Fig. 11, the parameter ϵ has to chosen according to the estimated platform dynamics. The previous attitude is stored in a "state buffer".

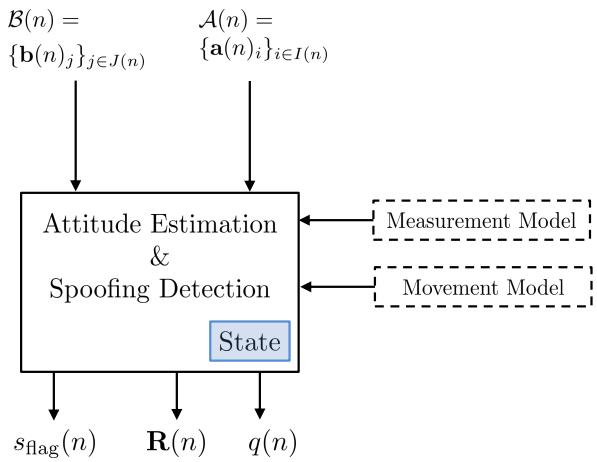

Fig. 11: Main block diagram of the sequential attitude estimator.

Mitigation

A robust spoofing detection scheme based on the sequential estimation of the array attitude has been presented in the

previous section. The attitude estimation problem at each estimation epoch is performed by using an SVD-based technique delivering closed-form solution for the problem. It is also shown that the spread of singular values can be used to detect anomalies in the measured satellite DoAs. These anomalies can be caused by the noise or structural interference, e.g. spoofing, and therefore can be used for detecting spoofing attacks. The practical use of this method for detecting the presence of the signals of a GPS repeater is illustrated by Fig. 17. In the figure it can be observed that in the presence of the repeater signals a single strong singular value prevails while the other two singular values are very close to zero.

The large spread between singular values obtained while solving for the antenna array attitude (see Equation 12) gives an indication that a strong correlation exists between the unit vectors of the measured DoAs in the matrix $\boldsymbol{B}$. In order to prove this a matrix $\boldsymbol{D} = \boldsymbol{B}^T\boldsymbol{B}$ of size $N \times N$ can be computed and tested for the non-diagonal elements close to unity. The non-diagonal elements are dot-products or cross-correlation factors between the different unit vectors of measured satellite DoAs. For a nominal satellite constellation these products are seldom close to unity since the presence of two or more satellites on the close positions in the sky is quite unlikely. In rare cases when this may nominally occur, a cross-check with the DoAs calculated from ephemeris or system almanac can be performed. If all checks above prove the anomaly condition, the direction of arrival of the structural interference can be estimated as the mean of the corresponding strongly correlated DoAs. The mitigation of the detected interference can then be performed by using a combination of a sub-space projection and eigenbeamforming [11] as described in the following part.

The estimated direction of the interference is described by an unit vector in $\mathbb{R}^3$. Before it can by applied for mitigation, this unit vector has to be projected into the antennas signalspace (see Fig.1). The mapping is specific for the geometry of the antenna. A generic description is given by $\mathcal{M} : \mathbb{R}^3 \mapsto \mathbb{C}^L$ where L corresponds to the number of antennas. The corresponding signal reads:

$$\boldsymbol{s}_{\text{RFI}} = \mathcal{M}(\boldsymbol{b}_{\text{RFI}}) \tag{22}$$

Subspace projection:

$$\boldsymbol{\Pi}^{\perp} = \boldsymbol{I} - \boldsymbol{s}_{\text{RFI}}(\boldsymbol{s}_{\text{RFI}}^H\boldsymbol{s}_{\text{RFI}})^{-1}\boldsymbol{s}_{\text{RFI}} \tag{23}$$

$$\boldsymbol{y} = \boldsymbol{\Pi}^{\perp}\boldsymbol{x} \tag{24}$$

where $\boldsymbol{\Pi}^{\perp} \in \mathbb{C}^{L\times L}$ is a sub-space projection matrix, and $\boldsymbol{x} \in \mathbb{C}^{L\times 1}$ and $\boldsymbol{y} \in \mathbb{C}^{L\times 1}$ are the array signal vectors before and after sub-space projection, correspondingly;

Eigenbeamforming:

$$\boldsymbol{C}_{\text{yy}} = E[\boldsymbol{y}\boldsymbol{y}^H] \tag{25}$$

$$y_{\text{BF}} = \boldsymbol{w}^H\boldsymbol{y} \tag{26}$$

where $\boldsymbol{C}_{\text{yy}} \in \mathbb{C}^{L\times L}$ is the array covariance matrix calculated after the sub-space projection, $\boldsymbol{w} \in \mathbb{C}^{L\times 1}$ is the eigenvector corresponding to the largest eigenvalue of the matrix $\boldsymbol{C}_{\text{yy}}$, $y_{\text{BF}} \in \mathbb{C}$ is the beamformers output that can be used by receiver tracking loops.

Experimental Results

The described methods are compared to the previous approaches in [9] and [7]. The same data set is available. A detailed description on how the data sets were collected can be found in the aforementioned references. All data sets where collected using DLR's multi-antenna GNSS receiver GALANT.

D. Nominal Case

The first data set was recorded placing GALANT antenna on the rooftop of the institute. Fig. 12 depicts the estimated attitude using the snapshot based approach compared to the iterative version in terms of absolute differences. Fig. 12 depicts the negligible difference, which is most likely caused by numerical effects.

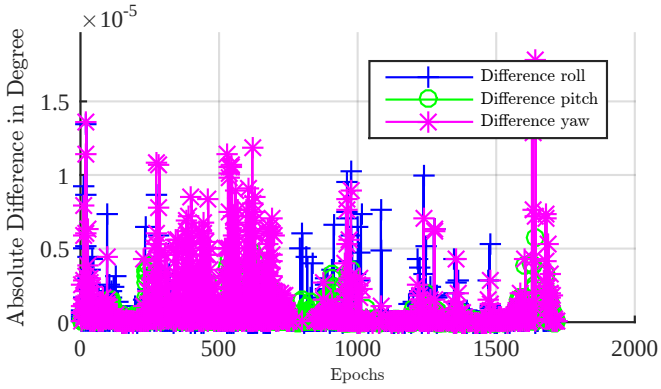

Fig. 12: Difference to iterative approach for the nominal case for roll, pitch and yaw.

The resulting SVD based quality metric for this nominal case is shown in Fig. 13. It is almost one for all periods, corresponding to a clean correlation between the almanac and measured DoAs.

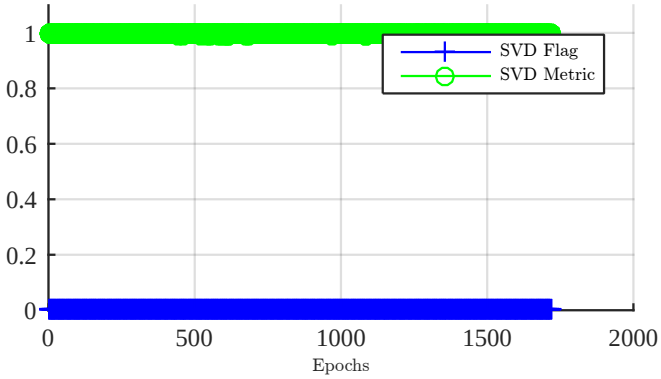

Fig. 13: SVD based quality metric for the nominal case.

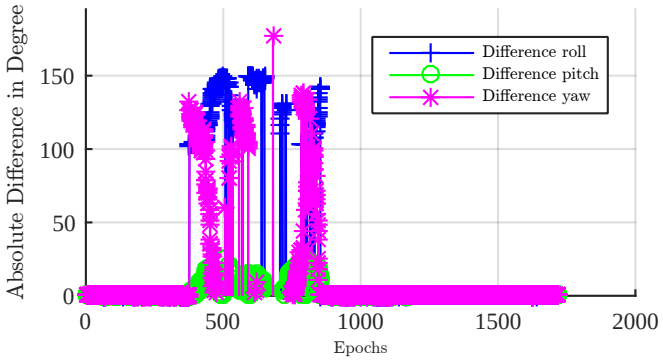

Fig. 14: Difference to iterative approach for the static repeater for roll, pitch and yaw.

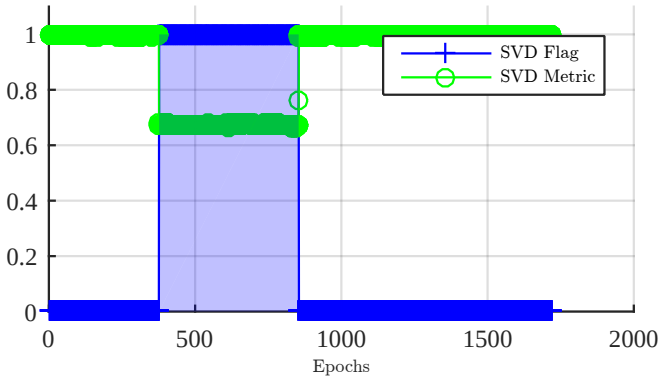

Fig. 15: SVD quality measurement (green) and spoofing flag (blue background).

E. Static Repeater

The repeater was realized connecting a GPS-L1 receiver antenna to a transmit antenna via an adjustable amplifier. The transmit antenna was attached to a balloon, which was fixed to ground, yielding a stationary setup.

The receiver under test was placed at a certain distance next to the balloon, allowing the reception of the nominal and repeated signals. The repeater was turned on after a certain period (epoch 376) and turned off (epoch 853) again.

The difference to the iterative approach is depicted in Fig. 14.

Differences are big in the time the repeater is turned on. The detection of that period is possible using the SVD based metric. The metric is depicted in Fig. 15. A blue background corresponds to a raised flag. The threshold was set to 0.8.

A comparison between the snapshot based approach and the smoothing approach is shown in Fig. 16. A slight loss in dynamic of the sequential version is recognizable.

In that case all signals are captured by the repeater, which is reflected by the distribution of the singular values shown in Fig. 17. The values are normalized by the number of available measurements for that time instant. Only one dominant singular value remains when the spoofer is turned on. As previously described, the corresponding left singular value corresponds to the spoofers direction in the local antenna frame and can be used for post-correlation nulling.

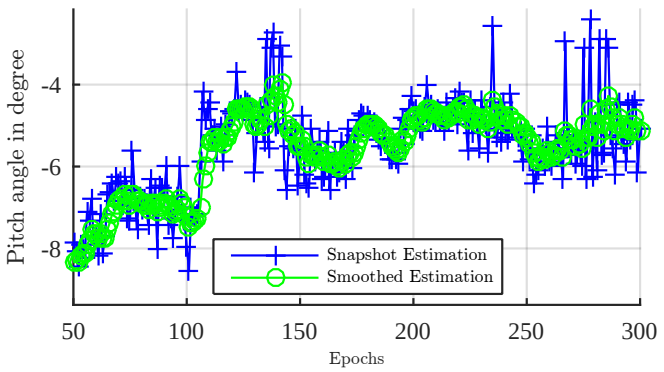

Fig. 16: Snapshot based approach compared to smoothing approach ($\epsilon = 1$).

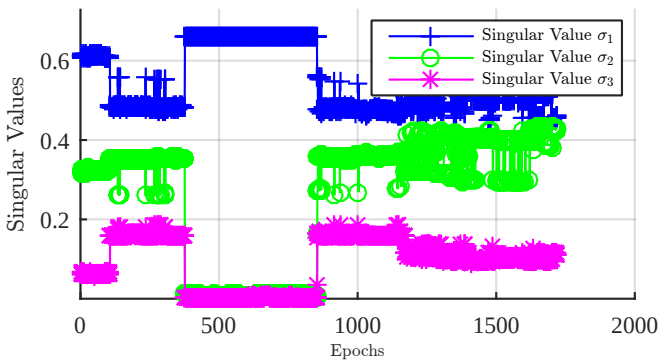

Fig. 17: Normalized singular values of the snapshot based approach.

F. Dynamic Repeater

The same setup was used as for the static case. The receiver under test was mounted on the rooftop of the measurement vehicle. The vehicle moved towards the repeater, turned and moved away again. The repeater was turned on all the time with constant transmit power (see [7] for more details and pictures).

Fig. 18 shows the difference compared to the iterative approach, which is high during the period the receiver is near the repeater (i.e. affected by the repeater).

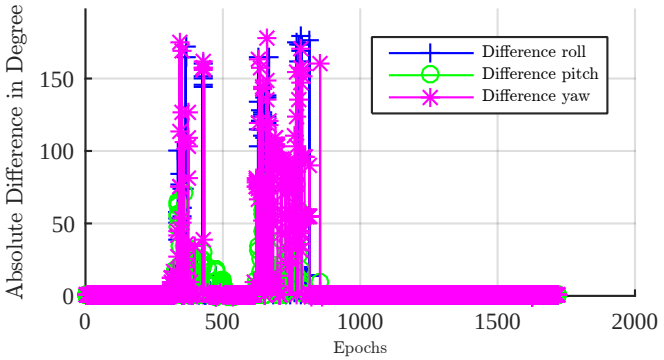

Fig. 18: Difference to iterative approach for the dynamic repeater for roll, pitch and yaw.

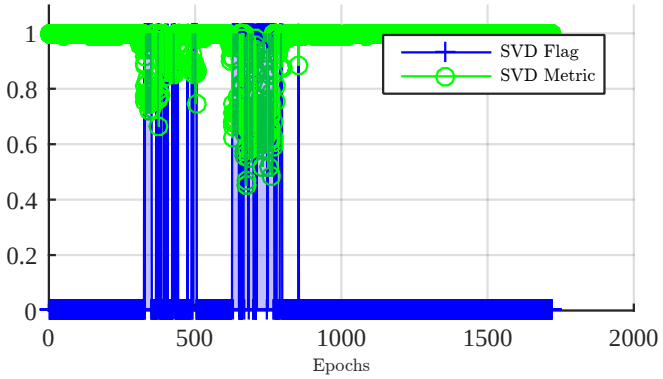

Fig. 19: SVD quality measurement (green) and spoofing flag (blue background).

Fig. 19 depicts the quality monitor and spoofing flag. Compared to the static case, no reliable threshold can be set.

Fig. 20 depicts the comparison for the yaw angle of the snapshot and smoothed approach. The missing modeling of higher order movement (i.e. yaw rate) limits the dynamics of the sequential estimator, whereas an estimate is calculated although the receiver is influenced by the repeater.

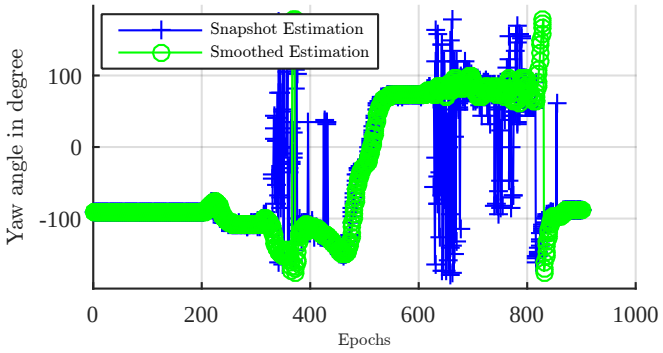

Fig. 20: Snapshot based approach compared to smoothing approach ($\epsilon = 1$).

The normalized singular values of the snapshot based approach are depicted in Fig. 21. In contrast to the static case, no clear dominant subspace can be identified.

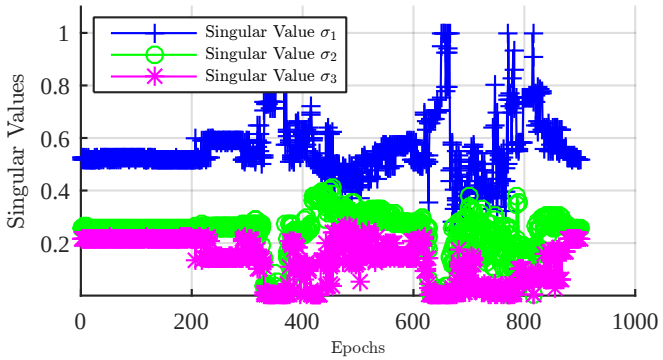

Fig. 21: Distribution of the normalized singular values.

Conclusion and Outlook

A computationally efficient algorithm has been developed exploiting the underlying geometry. Only one singular value decomposition per measurement is necessary, whereas the iterative approach of [9] uses one matrix inversion per iteration. An implementation in real time for DLR's multi-antanne receiver GALANT is currently performed.

Furthermore the results of the SVD can directly be used to inspect the quality of the measurements and current satellite geometry. A metric based on the strength of the correlation of the received and almanac based DoAs could be used in reliable way to test for anomalies, i.e. spoofing. The dominant subspace of the spoofer is directly given by the strongest left singular vector and can be used for mitigation at tracking level.

Finally a low complexity constraint based sequential estimator was presented. The overhead compared to the snapshot based approach is just one 3×3 matrix addition. Experimental data show a more robust behavior, although a certain latency is added.

Future work will focus on the following issues:

1) The practical verification of the proposed mitigation technique by implementing it in real time.
2) The offline calibration of the antenna array, to gain more accurate, i.e. unbiased, measurements for low elevations.
3) The extension of the sequential estimation to higher order movement models.
4) Estimation of the spoofers location in a local east-north-up coordinate frame.

Acknowledgment

Some parts of the research leading to the results reported in this paper have been funded by the program Research for Civil Security of the Federal Ministry of Education and Research (BMBF) of the Federal Republic of Germany under the grant FKZ 13N12744. Other aspects presented in this paper have been funded within the project KOSERNA by the German Aerospace Center (DLR) on behalf of the German Federal Ministry of Economics and Technology under grant nr 50 NA 1406. This support is greatly acknowledged.

References

[1] M. Appel, A. Hornbostel, and C. Haettich, "Impact of meaconing and spoofing on galileo receiver performance," *7th ESA Workshop on Satellite Navigation Technologies NAVITEC*, 2014.

[2] T. E. Humphreys, B. M. Ledvina, M. L. Psiaki, B. W. O'Hanlon, and P. M. Kintner Jr, "Assessing the spoofing threat: Development of a portable gps civilian spoofer," *Proceedings of the ION GNSS international technical meeting of the satellite division*, vol. 55, p. 56, 2008.

[3] K. Wesson, D. Shepard, and T. Humphreys, "Straight talk on anti-spoofing: Securing the future of pnt," *GPS World*, vol. 23, no. 1, 2012.

[4] A. Jafarnia-Jahromi, A. Broumandan, J. Nielsen, and G. Lachapelle, "Gps vulnerability to spoofing threats and a review of antispoofing techniques," *International Journal of Navigation and Observation*, vol. 2012, 2012.

[5] P. Y. Montgomery, T. E. Humphreys, and B. M. Ledvina, "A multi-antenna defense: Receiver-autonomous gps spoofing detection," *Inside GNSS*, vol. 4, no. 2, pp. 40–46, 2009.

[6] M. Meurer, A. Konovaltsev, M. Cuntz, and C. Hättich, "Robust joint multi-antenna spoofing detection and attitude estimation using direction assisted multiple hypotheses raim," 2012.

[7] A. Konovaltsev, S. Caizzone, M. Cuntz, and M. Meurer, "Autonomous spoofing detection and mitigation with a miniaturized adaptive antenna array," in *27th International Technical Meeting of the Satellite Division of The Institute of Navigation (ION GNSS+ 2014)*. The Institue of Navigation, USA, September 2014, pp. 2853–2861.

[8] M. Cuntz, L. Greda, M. Heckler, A. Konovaltsev, M. Meurer, L. Kurz, G. Kappen, and T. Noll, "Lessons learnt: The development of a robust multi-antenna gnss receiver," *Proc. ION GNSS 2010*, pp. 21–24, 2010.

[9] A. Konovaltsev, M. Cuntz, C. Haettich, and M. Meurer, "Performance analysis of joint multi-antenna spoofing detection and attitude estimation," in *ION International Technical Meeting 2013*, Januar 2013.

[10] D. Q. Huynh, "Metrics for 3d rotations: Comparison and analysis," *J. Math. Imaging Vis.*, vol. 35, no. 2, pp. 155–164, Oct. 2009.

[11] M. Sgammini, F. Antreich, L. Kurz, M. Meurer, and T. G. Noll, "Blind adaptive beamformer based on orthogonal projections for gnss," in *Proceedings of ION GNSS*, 2012.